Zhao et al. Nanoscale Research Letters (2017) 12:497
DOI 10.1186/s11671-017-2269-4

Nanoscale Research Letters

NANO EXPRESS Open Access

Photocatalytic Properties of Co_3O_4-Coated TiO_2 Powders Prepared by Plasma-Enhanced Atomic Layer Deposition

Xi-Rui Zhao, Yan-Qiang Cao, Jun Chen, Lin Zhu, Xu Qian, Ai-Dong Li* and Di Wu

Abstract

Co_3O_4-coated commercial TiO_2 powders (P25) p-n junction photocatalysts were prepared by plasma-enhanced atomic layer deposition (PEALD) technique. The structure, morphology, bandgap, and photocatalytic properties under ultraviolet light were investigated systematically. Although the deposition of Co_3O_4 does not change the anatase structure and crystallite size of P25 powders, the ultraviolet photocatalytic activity has been improved evidently. For the Co_3O_4-coated P25 powders, the trace Co ions exist as Co_3O_4 nanoparticles attached to TiO_2 powder surface instead of the occupation of Ti^{4+} position in TiO_2 lattice. The Co_3O_4-coated P25 powders exhibit enhanced photocatalytic degradation efficiency of almost 100% for methylene blue in 1.5 h under ultraviolet light, compared with P25 of 80%. The Mott-Schottky plots of photocatalyst powders confirm the p-n heterojunction formation in Co_3O_4–TiO_2 nanocomposite materials, which is beneficial to increase the efficiency of photogenerated electron-hole separation. In addition, the Co_3O_4 coating also promotes the adsorption of organic dyes of methylene blue on P25 powders.

Keywords: Plasma-enhanced atomic layer deposition, Commercial TiO_2 powders (P25), Surface modification, Co_3O_4, Photocatalytic acitivity, P-n junction

Background

With the rapid development of modern industry, water contamination has emerged as a serious issue [1, 2]. Organic dyes present toxic effects and reduce light penetration in contaminated water [3]. Moreover, most textile dyes show recalcitrance towards chemical oxidation and other traditional wastewater treatment. Fortunately, TiO_2-based photocatalysts exhibit excellent degradation towards organic dyes [4]. TiO_2 has been extensively and intensively studied as one of popular photocatalytic materials due to its low toxicity, high chemical stability, and catalytic activity in elimination of a large range of organic pollutants [5–7]. However, its overall quantum efficiency is relatively low due to the fast recombination rate of photogenerated electron-hole pairs [8]. Besides, the intrinsic large band gap of TiO_2 limits its optical absorption to the UV region, which only accounts for less than 4% of the total solar radiation [9, 10]. These flaws impede its practical applications. Hence, different approaches have been explored to improve its photocatalytic activities, including metal/nonmetal doping [11, 12], dye sensitization [13], and heterojunction formation [14, 15].

It has been demonstrated that building p-n heterojunction between n-type TiO_2 and p-type semiconductor, such as NiO or Ag_2O, is beneficial for reducing the recombination rate of photogenerated electrons and holes [16–18]. Firstly, the p-n junction can produce a built-in potential at the semiconductor interface. Under illumination, the inner electric field will promote the separation and transportation of photogenerated electron-hole pairs [19]. Secondly, semiconductors with smaller bandgap can enhance the light absorption of catalyst with larger bandgap [20]. Moreover, some semiconductors can also be employed to improve the stability of catalyst and facilitate the surface electrochemical reactions [21]. As a result, the photocatalytic activity could be improved dramatically by the formation of semiconductor/semiconductor hetero-junction. Chen et al. have reported that p-n

* Correspondence: adli@nju.edu.cn
National Laboratory of Solid State Microstructures and Department of Materials Science and Engineering, College of Engineering and Applied Sciences, Collaborative Innovation Center of Advanced Microstructures, Nanjing University, Nanjing 210093, People's Republic of China

junction NiO/TiO_2 photocatalyst showed improved photoactivity in degrading methylene blue (MB) [22].

Co_3O_4, one of the most versatile transition-metal oxides, is widely applied in many fields, such as dyes degradation [23, 24], gas sensors [25], lithium ion batteries [26], oxidation of CO at low temperature [27], and H_2 generation [28]. Co_3O_4, like NiO and Ag_2O, belongs to p-type semiconductors. Its bandgap (2.1 eV) is relatively narrower compared with that of NiO (3.5 eV). Moreover, it shows better chemical stability than Ag_2O because Ag_2O tends to absorb CO_2 in air to form Ag_2CO_3 or decomposes into Ag when used at a comparatively high temperature [28]. It has been reported that p-n $Co_3O_4/BiVO_4$ or Co_3O_4/TiO_2 junction exhibited higher photocatalytic activity than single semiconductor of $BiVO_4$ or TiO_2 in removing organic dyes [29, 30].

Quite a few methods have been used to synthesize Co_3O_4-based nanosystems, such as chemical vapor deposition (CVD) [31–33], plasma spray [34], and plasma-assisted CVD (PECVD) processes [35–37]. The Co_3O_4/TiO_2 p-n junction has also been fabricated by impregnating-deposition-decomposition method [30]. The subsequent calcination and excitation were needed, which might produce exhaust emission.

Atomic layer deposition (ALD) is a novel thin film deposition technique based on sequential self-limited and complementary surface chemisorption reactions using precursor vapor. Compared to CVD, PECVD, and chemical solution method, it exhibits unique advantages, including large area uniformity, excellent three-dimensional conformality, precise and simple control of film-thickness, flexible surface modification, and low processing temperature [38]. Plasma-enhanced atomic layer deposition (PEALD), where plasma species are employed as reactive gas during one step of the cyclic deposition process, shows some merits over thermal ALD, such as more freedom to the substrate temperature and precursors. Recently, ALD has shown increasing prospects and wide applications in various fields such as semiconductor [39], new energy [40], and photocatalysis [41], especially in the surface modification of nanomaterials [42].

Herein, trace Co_3O_4-coated TiO_2 p-n junction photocatalyst was fabricated by ALD method. Compared with the impregnating-deposition-decomposition method with multi-step procedures [30], ALD technique has only one-step deposition and low processing temperature of 200 °C without subsequent annealing. The crystal structure, morphology, composition, and bandgap of Co_3O_4-coated P25 powders were characterized by various analytical techniques. The photocatalytic activity of Co_3O_4-coated P25 powders with 100 and 200 cycles in the degradation of methylene blue (MB) dye under ultraviolet (UV) light irradiation has been investigated deeply. It can be found that, in contrast to the pure P25 powders, the 100-cycle Co_3O_4-coated P25 p-n junction sample exhibits distinctly enhanced UV photocatalytic efficiency. The possible photocatalytic mechanism of Co_3O_4-coated TiO_2 powders is also proposed.

Methods

Commercial TiO_2 powders (P25) were used as supporters for Co_3O_4 deposition. P25 powders were loaded uniformly into a porous container and placed in the PEALD chamber (SUNALE R-200, Picosun). Dicarbonyl cyclopentadienyl cobalt ($CoCp(CO)_2$, Strem Chemicals, 96%) kept at 45 °C and room-temperature oxygen plasma was used as cobalt precursor and oxygen source for Co_3O_4 deposition, respectively. High purity oxygen (99.999%) was used as oxygen plasma source with argon (99.999%) as carrier gas, and the plasma power and O_2 gas flow rate were 2500 W and 160 sccm, respectively. Then 100- and 200-cycle Co_3O_4 were deposited on P25 powders at 200 °C by PEALD, where one cycle consisted of 0.2 s $CoCp(CO)_2$ dosing, 6 s N_2 purging, 21.5 s O_2 plasma dosing, and 6 s N_2 purging. For the 600-cycle Co_3O_4-coated P25 sample, flowing oxygen (130 sccm) instead of oxygen plasma was used as oxygen source. The Co precursor and reactor temperature remained unchanged. Therefore, 600-cycle Co_3O_4 were deposited on P25 powders by thermal ALD, where one cycle consisted of 2 s $CoCp(CO)_2$ dosing, 8 s N_2 purging, 5 s O_2 dosing, and 10 s N_2 purging. In our previous work, it has been demonstrated that PEALD Co_3O_4 on carbon nanotubes showed a low deposition rate and island growth mode [43]. The thickness of 800- and 2400-cycle Co_3O_4 was 5 and 20 nm, respectively. The rough deposition surface was covered by Co_3O_4 nanoparticles. Therefore, 100- and 200- cycle Co_3O_4 deposition on P25 may be still in its nucleation stage, might leading to the formation of Co_3O_4 nanoparticles coated TiO_2 p-n junction structure.

The crystal structure of Co_3O_4-coated P25 powders was characterized by X-ray diffraction (XRD, Rigaku-D/max 2000) with Cu Kα radiation (λ = 0.15418 nm). The scanning angle ranged from 10° to 80° operated at 40 kV and 40 mA. The surface chemical feature was analyzed via X-ray photoelectron spectroscopy (XPS, Thermo ESCALAB-Thermo fisher K-alpha) using Al Kα radiation (1486.6 eV) as the excitation source. All binding energies were referenced to the C 1s peak at 284.6 eV. Inductively coupled plasma mass spectrometry (ICP-MS, Thermo X Series 2 ICP-MS) was carried out to measure the Co element content of photocatalyst powders.

The microstructure and surface morphology of the powders were characterized using field-emission scanning electron microscopy (FESEM, Ultra 55, ZRISS) and transmission electron microscopy (TEM, FEI Tecnai G^2 F20 S-Twin). The catalyst powders were dispersed fully in ethanol by 20 min ultrasonic vibration before

dripping onto the copper grid with ultrathin carbon foil for TEM observation. The Brunauer-Emmett-Teller (BET) specific surface areas were carried out using nitrogen adsorption apparatus (Micromeritics Tristar-3000).

The photocatalytic activity of Co_3O_4-coated TiO_2 powders in the decomposition of methylene blue (MB) was evaluated under irradiation of a 100-W UV LED lamp (UVEC-411). Circulating cooling water was employed to maintain the system temperature at ~ 25 °C. The lamp was located at 15 cm away from the reaction solution. Fifty milligrams of catalyst was added into 50 mL MB aqueous solution (37.4 mg/L). Prior to the illumination, the mixed solution was stirred for 3 h in the absence of light to achieve the adsorption equilibrium. After each given irradiation time, about 4 mL of the mixture was withdrawn and separated by centrifuging to remove the suspended solid catalyst. The degradation process was monitored by a UV-vis absorption spectrum (UV-3600, Shimadzu, Japan), and the concentration of the residual MB was analyzed quantitatively by measuring the maximum absorption at 664 nm.

The visible-light photocatalytic activity of Co_3O_4-coated TiO_2 powders was also evaluated via the degradation of methyl orange (MO) in aqueous solution. A solar simulator (300 W Xe lamp, MircoSolar300, PerfectLight) with a 420-nm cut-off filter provides the visible-light irradiation. The concentration of residual MO was determined by measuring the maximum absorption of MO at 464 nm.

Mott-Schottky plots were measured using electrochemical working station (CHI Instruments CHI760E) at frequencies of 1 and 2 kHz in dark. Fifty-two-milligram P25 or 200-cycle Co_3O_4-coated P25 powders along with 18 mg iodine were dispersed in 50 mL acetone via ultrasonic vibration. Then, the mixed slurry was electroplated onto fluorine-doped tin oxide (FTO) conducting glass under 15 V for 2 min. The electrochemical measurement was conducted in 1 M NaOH electrolyte at room temperature using a three-electrode configuration. The as-prepared FTO glass with photocatalyst was adopted as the working electrode. A platinum mesh (1 cm × 2 cm) and Ag/AgCl were used as counter electrode and reference electrode, respectively. The isoelectric point (IEP) of MB, P25, and 200-cycle Co_3O_4-coated P25 in aqueous solutions was determined using the Zeta potential measurement (Malvern Zetasizer, Nano ZS 90 zeta).

Results and Discussion

XRD was used to determine the phase structure of the samples. Figure 1 exhibits the XRD patterns of pure P25 and 200-cycle Co_3O_4-coated P25 powders. Both samples display the similar characteristic peaks of standard anatase TiO_2 (JCPDS card no: 21–1272), suggesting that there is no obvious change in the crystal structure after Co_3O_4 coating. In addition, the crystallite size of both samples can be estimated to be 20 ± 2 nm by Scherrer formula.

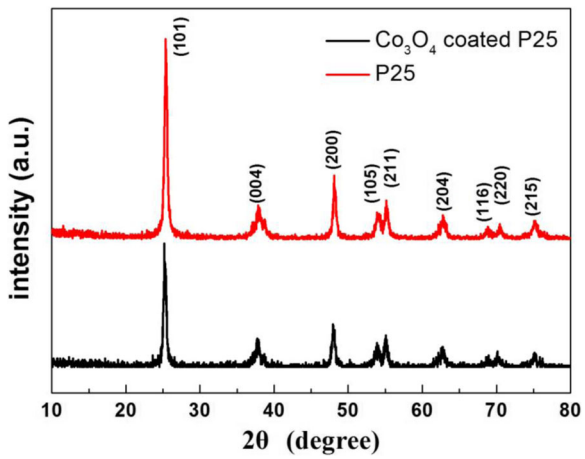

Fig. 1 XRD patterns of pure P25 and 200-cycle Co_3O_4-coated P25 powders

SEM and TEM were utilized to observe the morphology and microstructure of pure P25 and 200-cycle Co_3O_4-coated P25 powders, as shown in Fig. 2a–d. Pure P25 and 200-cycle Co_3O_4-coated P25 samples show similar morphology and crystallite size of 15–30 nm (Fig. 2a, b). The nanoparticle size distribution was also counted, as shown in Fig. 2e, f, which can be fitted to Gaussian curves. The calculated average value of crystallite sizes of pure P25 and 200-cycle Co_3O_4-coated P25 powders is ~ 25.8 and ~ 26.2 nm, respectively, which is slightly larger than the XRD result due to the easy negligence of smaller nanoparticles in SEM observations. These nanoparticles agglomerate together to form some larger clusters of 50–100 nm. In high-resolution TEM (HRTEM) image of Fig. 2c, a local magnification well-crystallized TiO_2 nanocrystal with clear lattice fringes can be seen in pure P25 powders. After 200-cycle PEALD Co_3O_4, we can notably discern some small amorphous nanoparticles located on the larger crystalline TiO_2 surface with the diameter of 2–3 nm, as marked by arrows in Fig. 2d. Based on our previous work [43], these small nanoparticles should be the PEALD-derived Co_3O_4 with island growth mode. Combined with TEM and XRD results, it can be deduced that the Co ions exist as Co_3O_4 amorphous nanoparticles attached to TiO_2 powder surface instead of the occupation of Ti^{4+} position in TiO_2 lattice.

In addition, the influence of PEALD Co_3O_4 on the specific surface area of P25 was also examined. The BET surface area is 112.6 and 104.0 m^2/g for pure P25 and Co_3O_4-coated P25 powders, respectively, so Co_3O_4 deposition on P25 powders has slight effect on the specific surface area of P25.

XPS was performed to investigate the chemical composition of the samples with and without PEALD 100-cycle

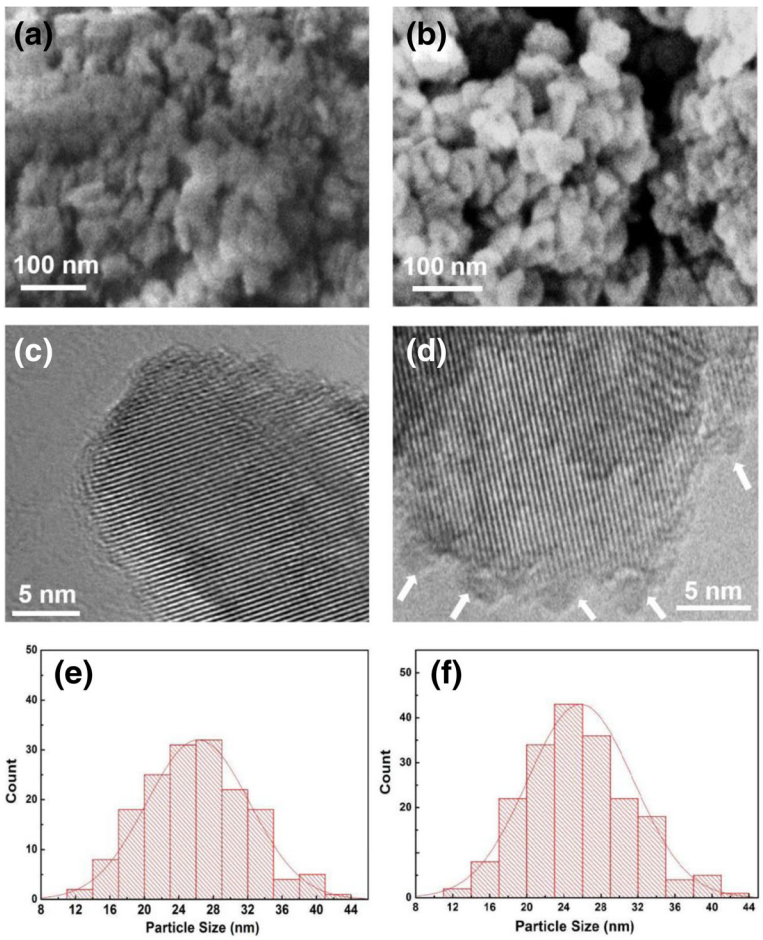

Fig. 2 SEM (**a**, **b**) and HRTEM (**c**, **d**) images of pure P25 and 200-cycle Co_3O_4-coated P25 powders along with the particle size distribution (**e**, **f**). **a**, **c**, **e** Pure P25 powders. **b**, **d**, **f** 200-cycle Co_3O_4-coated P25 powders

Co_3O_4 coating. Both samples show nearly the same signals for Ti 2p and O 1s spectra. In Fig. 3a, the doublet at 464.6 and 458.9 eV can be assigned to Ti^{4+} $2p_{1/2}$ and Ti^{4+} $2p_{3/2}$ peaks of Ti–O bonds with the spin orbit splitting energy of 5.7 eV, consistent with the values of TiO_2. The O 1s spectra can be deconvoluted into two peaks, as shown in Fig. 3b. The strong peak at 529.9 eV can be assigned to the O–Ti bond. The weak peak with higher binding energy at 532.2 eV is attributed to the absorbed OH species on the sample surfaces [44]. The O1s peak of Co_3O_4 should locate at ~ 529.8 eV [43], which is difficult to be distinguished from the O–Ti bond. The calculated atomic ratio of Ti:O is about 1.00: 2.13, basically consistent with the composition of TiO_2. However, the Co signal of 100-cycle Co_3O_4-

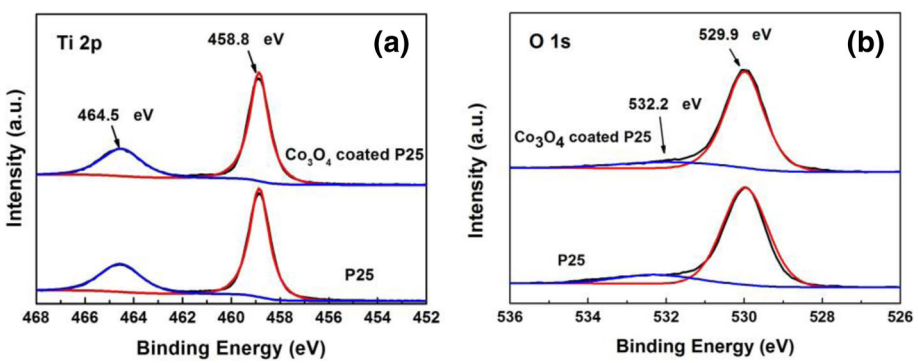

Fig. 3 XPS spectra of 100-cycle Co_3O_4-coated P25 powders and pure P25 powders. **a** Ti 2p. **b** O 1s

coated P25 powders is too weak to be detected. It can be ascribed to the fact that Co content may be below the detection limit of XPS. Therefore, ICP-MS was utilized to determine the Co content in pure P25 and 100-cycle Co_3O_4-coated P25 powders. It is found that Co content in pure P25 and 100-cycle Co_3O_4-coated P25 is 0.13 and 3.63 ppm, respectively. Hence, trace Co_3O_4 is indeed deposited on the P25 powders by PEALD. In addition, XPS was also used to analyze 600-cycle Co_3O_4-coated P25 samples prepared by thermal ALD. The weak Co 2p spectra can be recognized with the Co atomic percentage content of ~ 0.6%.

Figure 4a records the room-temperature UV-visible diffuse reflection spectra of pure P25 and Co_3O_4-coated P25 samples with 200 and 600 cycles. Pure P25 and 200-cycle Co_3O_4-coated P25 samples show almost the same optical absorption spectra, however, 600-cycle Co_3O_4-coated P25 samples derived from thermal ALD exhibit relatively stronger absorption in the visible range from 400 to 700 nm, especially in 400–500 nm region, which originates from the d-d transition for Co^{3+} or Co^{2+} ions.

For the direct bandgap semiconductor, the relation between the absorption edge and the photon energy ($h\nu$) can be written as follows [45]:

$(\alpha h\nu)^2 = A(h\nu - E_g)$ where A is the absorption constant of the direct band gap semiconductor. The absorption coefficient (α) is determined from the scattering and reflectance spectra according to Kubelka-Munk theory. The direct bandgap energies can be estimated from the intercept of the tangents to the plots, as presented in Fig. 4b. The bandgap of 200-cycle Co_3O_4-coated P25 powders is about 3.41 ± 0.02 eV, almost the same as pure TiO_2 powders (3.38 ± 0.02 eV), due to extremely low Co loading amount (~ppm by ICP-MS). Six hundred-cycle Co_3O_4-coated P25 samples show two bandgaps because of relatively higher Co loading (~ 0.6 atomic % by XPS). The larger bandgap of 3.20 ± 0.03 eV comes from TiO_2 powders, whereas the much smaller bandgap of 2.47 ± 0.03 eV might be related to Co_3O_4 coating. ALD-derived Co_3O_4 coating has slightly wider bandgap than the literature value of 2.3 eV from Co_3O_4 nanospheres (~ 20 nm) by solution-based synthesis [46].

MB is commonly used as the probe for evaluating photocatalysts, and its degradation mechanism has been well clarified. Figure 5a–c illustrates the photocatalytic decomposition of MB under UV light in the presence of pure P25, 100-cycle, and 200-cycle Co_3O_4-coated P25 photocatalysts, respectively. The maximum absorption of MB is located at 664 nm. The absorption intensity decreases with time under UV light irradiation for all the samples, corresponding to the degradation of MB. Figure 5d plots the photocatalytic degradation curves for all the samples. Both pure P25 and Co_3O_4-coated P25 powders can degrade MB under UV light. Meanwhile, almost no degradation of MB is observed in UV light without catalyst, demonstrating that MB is stable under UV light. However, 100- or 200-cycle Co_3O_4-coated P25 powders show much higher photocatalytic activity compared to pure P25 powders. The degradation efficiency of Co_3O_4-coated P25 can reach nearly 100% in 1.5 h, while that of the pure P25 is only about 80%.

The recycling tests were also carried out to determine the stability of the composite catalysts of Co_3O_4-coated P25 powders. No decay of photocatalytic efficiency is observed in 200-cycle Co_3O_4-coated P25 samples after repeatedly used in MB photodegradation for three times.

The enhanced photocatalytic activity of Co_3O_4-coated P25 powders could be attributed to the formation of p-n junction between Co_3O_4 and TiO_2. Figure 6 records Mott-Schottky plots of P25 with or without 200-cycle Co_3O_4 coating. Pure P25 samples exhibit the Mott-Schottky plot with positive slope, suggesting the n-type semiconductor with electron carriers. The Mott-Schottky plot with negative slope implies the p-type semiconductor with hole carriers. For 200-cycle Co_3O_4-coated P25 catalyst, the co-existence of positive and negative slopes with similar values in the Mott-Schottky plot can be simultaneously observed, indicating the formation of the p-n

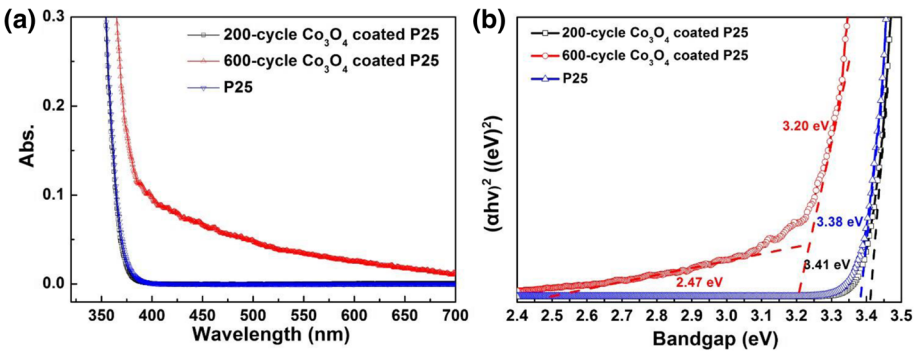

Fig. 4 **a** UV-visible diffuse reflection spectra and (**b**) corresponding band gaps determination plots of pure P25, 200-cycle and 600-cycle Co_3O_4-coated P25 powders

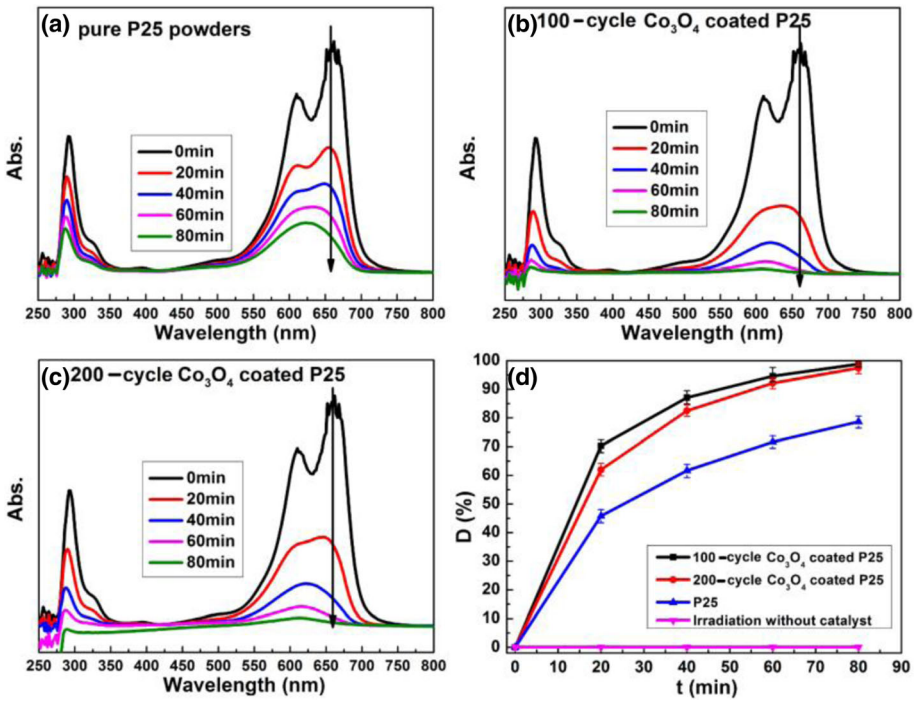

Fig. 5 UV-visible absorption and degradation curves of MB solution with various catalysts. **a** Pure P25. **b** 100-cycle Co_3O_4. **c** 200-cycle Co_3O_4-coated P25 catalyst. **d** Degradation curves of MB

junction in our samples. This will help in the separation of photogenerated electron-hole pairs [18, 22, 47].

Figure 7 illustrates the schematic of energy level and electron-hole movement in Co_3O_4–TiO_2 p-n junction structure. Co_3O_4 exhibits a much smaller band gap (~2.4 eV) than TiO_2 (~3.4 eV). Upon ultraviolet light irradiation, electron-hole pairs can be generated in both Co_3O_4 and TiO_2. According to the energy level structure in Fig. 7, photogenerated electrons would move from conduction band of Co_3O_4 to that of TiO_2. In contrast, holes are injected from the valence band of TiO_2 to that of Co_3O_4. As a result, a high concentration of electrons and holes are formed in the conduction band of TiO_2 and valence band of Co_3O_4, respectively. The electron-hole pair recombination is effectively hindered due to the separation of photogenerated electrons and holes.

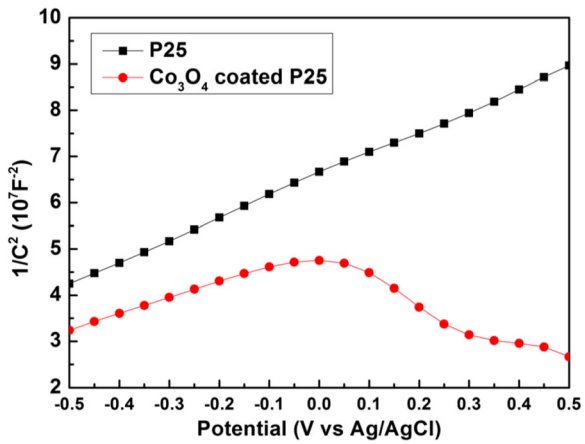

Fig. 6 Mott-Schottky plots of pure P25 and Co_3O_4-coated P25 in 1 M NaOH aqueous solution with frequencies of 1 and 2 kHz in the dark

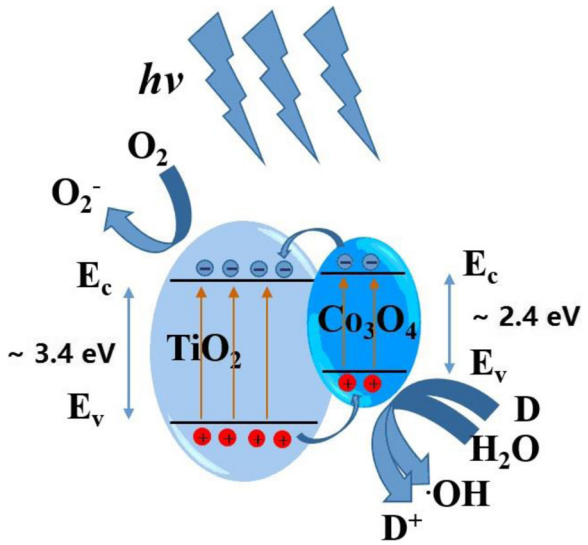

Fig. 7 Schematic of energy level and electron-hole movement in Co_3O_4–TiO_2 p-n junction structure under UV light irradiation

The separated electrons and holes are then free to undergo reactions with the reactants adsorbed on the photocatalyst surface and enhance the photocatalytic activity. Therefore, the Co_3O_4–TiO_2 p-n junction structure exhibits the better photocatalytic property than pure TiO_2.

In addition, in order to evaluate the influence of the isoelectric point (IEP) on the absorption of MB, the IEP was detected using the Zeta potential measurement, as shown in Fig. 8. The IEP of MB, pure P25, and 200-cycle Co_3O_4-coated P25 in aqueous solutions are determined to be 5.37, 6.74, and 7.42, respectively. The pH value of MB dye and P25 or Co_3O_4-coated P25 aqueous suspension is measured to be 6.68. According to the IEP results, the MB dye carries net negative charge while both catalysts carry positive charge. Moreover, Co_3O_4-coated P25 powders have more positive charges than pure P25. Therefore, the Co_3O_4 coating could promote the adsorption of MB on P25, which is beneficial to the enhancement of photocatalytic activity.

Finally, the photo-degradation test of methyl orange (MO) using Co_3O_4-coated P25 powders was also conducted under visible light illumination. The 200-cycle Co_3O_4-coated P25 sample shows no photocatalytic activity for degradation of MO. It can be ascribed to the fact that there exists only trace Co_3O_4 on the P25 surface. The trace Co_3O_4 cannot absorb enough visible light to stimulate the catalytic reactions. Therefore, we prepared 600-cycle Co_3O_4-coated P25 sample by thermal ALD to introduce more Co_3O_4 nanoparticles onto P25 powders. The photocatalytic activity in decomposition of MO dye has been examined under visible light irradiation ($\lambda \geq 420$ nm), as recorded in Fig. 9. Six hundred-cycle Co_3O_4-coated P25 shows visible photocatalytic activity with degradation of ~ 26% MO in 120 min. This can be explained by considering the Co_3O_4 nanoparticles activity under visible light due to its narrow bandgap (~ 2.4 eV) as confirmed by Fig. 4d [28].

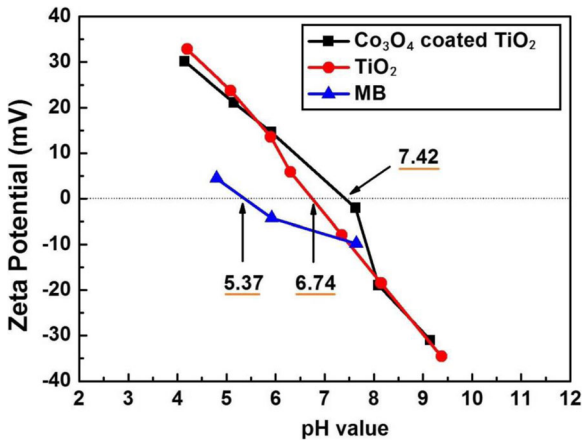

Fig. 8 Zeta potential of MB, P25, and Co_3O_4-coated P25 in aqueous solutions as a function of pH values

Conclusions

In summary, Co_3O_4-coated P25 p-n junction powder photocatalysts have been successfully prepared by PEALD. The structure, morphology, composition, and bandgap of these modified P25 powders have been characterized systematically. The photocatalytic activity of MB degradation under UV light has been explored deeply. The anatase structure and crystallite size of P25 powders do not change after 100- and 200-cycle Co_3O_4 deposition. However, under UV light, the Co_3O_4-coated P25 powders exhibit the degradation rate of almost 100% in 1.5 h. The UV photocatalytic activity has been evidently enhanced compared with pure P25 powders. The Mott-Schottky plots of photocatalyst powders confirm the p-n heterojunction formation in Co_3O_4–TiO_2 nanocomposite materials, which is beneficial to the separation of photogenerated electron-hole pairs. In addition, the IEP results also indicate that the Co_3O_4 coating could promote the adsorption of organic dyes of methylene

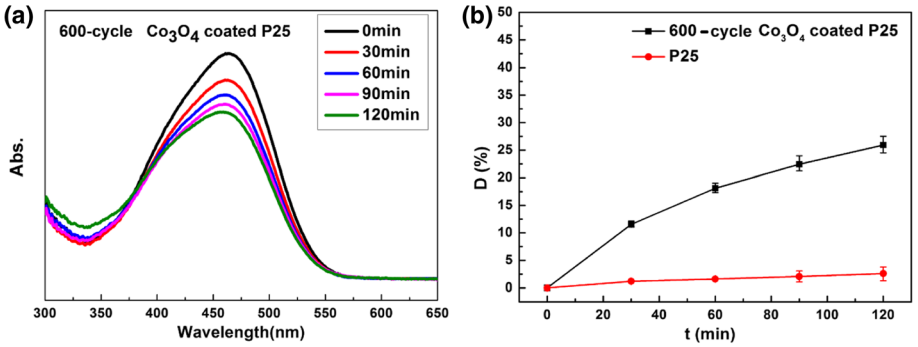

Fig. 9 Visible photocatalytic activity of 600-cycle Co_3O_4-coated P25 powders. **a** UV-visible absorption and **b** degradation curves of MO solution under visible light irradiation

blue on P25 powders. Above all, ALD is a promising and powerful technology to construct effective p-n junction photocatalyst via surface modification.

Acknowledgements
This project is supported by the Natural Science Foundation of China and Jiangsu Province (51571111, BK2016230, and BK20170645), a grant from the State Key Program for Basic Research of China (2015CB921203). Dr. Yan-Qiang Cao also thank the support from the general grant from the China Postdoctoral Science Foundation (2017M611778) and the Fundamental Research Funds for the Central Universities (021314380075).

Authors' Contributions
XRZ and JC carried out the sample fabrication and photodegradation measurements. XRZ drafted the manuscript. XRZ and YQC did the data analysis and interpreted the results. XRZ and XQ finished the TEM sample preparation and observation. LZ performed the SEM observation. ADL and DW participated in the discussion of the results. ADL supervised the whole work. CYQ and ADL revised the manuscript. All authors critically read and commented on the manuscript. All authors read and approved the final manuscript.

Competing Interests
The authors declare that they have no competing interests.

Publisher's Note

Received: 29 May 2017 Accepted: 7 August 2017
Published online: 16 August 2017

References

1. Daghrir R, Drogui P, Robert D (2013) Modified TiO_2 for environmental photocatalytic applications: a review. Ind Eng Chem Res 52:3581–3599
2. Anpo M, Dohshi S, Kitano M, Hu Y, Takeuchi M, Matsuoka M (2005) The preparation and characterization of highly efficient titanium oxide-based Photofunctional materials. Annu Rev Mater Res 35:1–27
3. Prado A, Bolzon L, Pedroso C, Moura A, Costa L (2008) Nb_2O_5 as efficient and recyclable photocatalyst for indigo carmine degradation. Appl Catal B Environ 82:219–224
4. Arslan I, Balcioglu AI (2001) Advanced oxidate of rawand biotreatedtextile industry wastewater with O_3, H_2O_2/UV-C and their sequential application. J Chem Technol Biotechnol 76:53–60
5. Khataeea A, Kasiri M (2010) Photocatalytic degradation of organic dyes in the presence of nanostructured titanium dioxide: influence of the chemical structure of dyes. J Mol Catal A Chem 328:8–26
6. Tachikawa T, Zhang P, Bian Z, Majima T (2014) Efficient charge separation and photooxidation on cobalt phosphate-loaded TiO_2 Mesocrystal superstructures. J Mater Chem A 2:3381–3388
7. Banisharif A, Khodadadi A, Mortazavi Y, Firooz A, Beheshtian J, Agah S, Menbari S (2015) Highly active Fe_2O_3-doped TiO_2 photocatalyst for degradation of trichloroethylene in air under UV and visible light irradiation: experimental and computational studies. Appl Catal B Environ 165:209–221
8. Chen J, Qiu F, Xu W, Cao S, Zhu H (2015) Recent progress in enhancing photocatalytic efficiency of TiO_2-based materials. Appl Catal A General 495:131–140
9. Tong H, Ouyang S, Bi Y, Umezawa N, Oshikuri M, Ye J (2012) Nano-photocatalytic materials: possibilities and challenges. Adv Mater 24:229–251
10. Dong H, Zeng G, Tang L, Fan C, Zhang C, He X, He Y (2015) An overview on limitations of TiO_2-based particles for photocatalytic degradation of organic pollutants and the corresponding countermeasures. Water Res 79:128–146
11. Kontos A, Likodimos V, Stergiopoulos T, Tsoukleris D, Falaras P (2009) Self-organized anodic TiO_2 nanotube arrays functionalized by iron oxide nanoparticles. Chem Mater 21:662–672
12. Yuan S, Mu J, Mao R, Li Y, Zhang Q, Wang H (2014) All-nanoparticle self assembly ZnO/TiO_2 heterojunction thin films with remarkably enhanced photoelectrochemical activity. ACS Appl Mater Interfaces 6:5719–5725
13. Aslan E, Gonce M, Yigit M, Sarilmaz A, Stathatos E, Ozel F, Can M, Patir I (2017) Photocatalyc H_2 evolution with a Cu_2WS_4 catalyst on a metal free D-π-a organic dye-sensitized TiO_2. Appl Catal B Environ 210:320–327
14. Scuderi V, Amiard G, Sanz R, Boninelli S, Impellizzeri G, Privitera V (2017) TiO_2 coated CuO nanowire array: ultrathin p-n heterojunction to modulate cationic/anionic dye photo-degradation in water. Appl Surf Sci 416:885–890
15. Boumaza S, Bellal B, Boudjemaa A, Trari M (2016) Photodegradation of Orange G by the hetero-junction x% Bi_2S_3/TiO_2 under solar light. Sol Energy 139:444–451
16. Wang M, Hu Y, Han J, Guo R, Xiong H (2015) TiO_2/NiO hybrid shells: p-n junction photocatalysts with enhanced activity under visible light. J Mater Chem A 3:20727–20735
17. Sampath S, Maydannik P, Ivanova T, Shestakova M, Homola T, Bryukvin A, Silanpaa M, Nagumothu R, Alagan V (2016) Efficient solar photocatalytic activity of TiO_2, coated nano-porous silicon by atomic layer deposition. Superlattice Microst 97:155–166
18. Kumar D, Reddy N, Karthik M, Karthik M, Neppolian B, Madhavan J, Shankar M (2016) Solar light sensitized p-Ag_2O/n-TiO_2, nanotubes Heterojunction Photocatalysts for enhanced hydrogen production in aqueous-glycerol solution. Sol Energy Mater Sol Cells 154:78–87
19. Wang C, Thompson R, Ohodnicki P, Baltrus J, Matranga C (2011) Size-dependent photocatalytic reduction of CO_2 with PbS quantum dot sensitized TiO_2 heterostructured photocatalysts. J Mater Chem 21:13452–13457
20. In S, Dimitri D, Vaughn II, Schaak R (2012) Hybrid CuO-$TiO_{(2-x)}N_{(x)}$ hollow nanocubes for photocatalytic conversion of CO_2 into methane under solar irradiation. Angew Chem Int Ed 51:3915–3918
21. Chen X, Shen S, Guo L, Mao S (2010) Semiconductor-based photocatalytic hydrogen generation. Chem Rev 110:6503–6570
22. Chen C, Liao C, Hsu K, Wu Y, Wu J (2011) P-N junction mechanism on improved NiO/TiO_2 Photocatalyst. Catal Commun 12:1307–1310
23. P. Raja, M. Bensimon, U.Klehm, P. Albers, D. Laub, L. Minsker-Kiwi, A. Renken, J, Kiwi, J. Photochem (2007) Highly dispersed PTFE/Co_3O_4 flexible films as Photocatalyst showing fast kinetic performance for the discoloration of Azo-dyes under solar irradiation. J Photochem & Photobio A Chem 187: 332-338
24. Yu Z, Bensimon M, Laub D, Kiwi-Minsker L, Jardim W, Mielczarski E, Mielczarski J, Kiwi J (2007) Accelerated photodegradation (minute range) of the commercial Azo-dye Orange II mediated by Co_3O_4/Raschig rings in the presence of oxone. Jour Mol Catal A Chem 272:11–19
25. Choi K, Kim H, Kim K, Li D, Cao G, Lee J (2010) C_2H_5OH sensing characteristics of various Co_3O_4 nanostructures prepared by solvothermal reaction. Sensors Actuators B Chem 146:183–189
26. Guo B, Li C, Yuan Z (2010) Nanostructured Co_3O_4 materials: synthesis, characterization and electrochemical behaviors as anode reactants in rechargeable lithium ion batteries. J Phys Chem C 114:12805–12817
27. Hu L, Peng Q, Li Y (2008) Selective synthesis of Co_3O_4 nanocrystal with different shape and crystal plane effect on catalytic property for methane combustion. J Am Chem Soc 130:16136–16137
28. Gasparotto A, Barreca D, Bekermann D, Devi A, Fischer R (2011) F-doped Co_3O_4 photocatalysts for sustainable H_2 generation from water/ethanol. J Amer Chem Soc 133:19362–19365
29. Long M, Cai W, Cai J, Zhou B, Chai A (2006) Efficient photocatalytic degradation of phenol over Co_3O_4/$BiVO_4$ composite under visible light irradiation. ChemInform 110:20211–20216
30. Dai G, Liu S, Liang Y, Luo T (2013) Synthesis and enhanced photoelectrocatalytic activity of p-n junction Co_3O_4/TiO_2 nanotube arrays. Appl Surf Sci 264:157–161
31. Barreca D, Cruz-Yusta M, Gasparotto A, Maccato C, Morales J, Pozza A, Sada C, Sanchez L, Tondello E (2010) Cobalt oxide Nanometerials by vapor-phase synthesis for fast and reversible lithium storage. J Phys Chem C 114:10054–10060
32. Barreca D, Fornasiero P, Maccato C, Pozza A, Tondello E (2010) CVD Co_3O_4 nanopyramids: a nano-platform for photo-assisted H_2 production. Chem Vap Depos 16:296–300
33. Barreca D, Comini E, Gasparotto A, Maccato C, Pozza A, Sada C, Sberveglieri G, Tondello E (2010) Vapor phase synthesis, characterization and gas sensing performances of Co_3O_4 and au/Co_3O_4 nanosystems. J Nanosci Nanotechnol 10:8054–8061
34. Tummala R, Guduru R, Mohanty P (2012, 209) Nanostructured Co3O4 electrodes for supercapacitor applications from plasma spray technique. J Power Sources:44–51
35. Barreca D, Bekermann D, Comini E, Devi A, Fischer R, Gasparotto A, Gavagnin M, Maccato C, Sada C, Sberveglieri G, Tondello E (2011) Plasma enhance-CVD of

undoped and fluorine-doped Co_3O_4 nanosystems for novel gas sensors. Sensors Actuators B 160:79–86
36. Barreca D, Devi A, Fischer R, Bekermann D, Gasparotto A, Gavagnin M, Maccato C, Tondello E, Bontempi E, Depero L, Sada C (2011) Strongly oriented Co_3O_4 thin films on MgO (100) and $MgAl_2O_4$ (100) substrates by PE-CVD. CrystEngComm 13:3670–3673
37. Tyczkowski J, Kapica R, Lojewska J (2007) Thin cobalt oxide films for catalysis deposited by plasma-enhanced metal-organic chemical vapor deposition. Thin Solid Films 515:6590–6595
38. Lim BS, Rahtu A, Gordon RG (2003) Atomic layer deposition of transition metals. Nat Mater 2:749
39. Martinson ABF, Elam JW, Pellin MJ, Univ N (2009) Atomic layer deposition of CuS for future application in photovoltaics. Appl Phys Lett 94:123107–123107-3
40. Marichy C, Bechelany M, Pinna N (2012) Atomic layer deposition of nanostructured materials for energy and environmental applications. Adv Mater 24:1017–1032
41. Cao Y, Chen J, Zhou H, Zhu L, Li X (2015) Photocatalytic activity and photocorrosion of atomic layer deposited ZnO ultrathin films for the degradation of methylene blue. Nanotechnology 26:024002
42. Mackus A, Bol A, Kessels W (2014) The use of atomic layer deposition in advanced nanopatterning. Nano 6:10941–10960
43. Guan C, Qian X, Wang X, Cao Y, Zhang Q, Li A, Wang I (2015) Atomic layer deposition of Co_3O_4 on carbon nanotubes/carbon cloth for high-capacitance and ultrastable supercapacitor electrode. Nanotechnology 26:5017–5024
44. Fittipaldi M, Gombac V, Gasparotto A, Deiana C, Adami G, Barreca D, Montini T, Martra G, Gatteschi D, Fornasiero P (2011) Synergistic role of B and F dopants in promoting the photocatalytic activity of rutile TiO_2. ChemPyhsChem 12:2221–2224
45. Raoufi D, Raoufi T (2009) The effect of heat treatment on the physical properties of sol–gel derived ZnO thin films. Appl Surf Sci 255:5812–5817
46. Li Y, Zhao J, Zhao Y, Hao X, Hou Z (2013) Facile solution-based synthesis and optical properties of Co_3O_4 Nanoparticles at low-temperature. Chem Res Chin Univ 29:1040–1044
47. Li J, Meng F, Suri S, Ding W, Huang F, Wu N (2012) Photoelectrochemical performance enhance by a nickel oxide-hematite p-n junction photoanode. ChemComm 48:8213–8215